actuators

MDPI

Article

Semi-Active Vibration Control of Automotive Subframes and Seats Using Magnetorheological Elastomer Actuators

Yuta Sobue [1], Yusaku Yamada [1], Yudai Kawase [2], Rafid Newaj Arefin [1] and Osamu Terashima [2,*]

[1] Graduate School of Natural Science and Technology, Gifu University, 1-1 Yanagido, Gifu 501-1193, Japan
[2] Faculty of Mechanical Systems Engineering, Gifu University, 1-1 Yanagido, Gifu 501-1193, Japan
* Correspondence: terashima.osamu.e0@f.gifu-u.ac.jp

Abstract

Magnetorheological elastomers (MREs) exhibit magnetic-field-dependent stiffness and can, therefore, be used to tune the natural frequency of a dynamic vibration absorber through the applied coil current. This study evaluates the extension of a previously developed MRE-based semi-active absorber to two automotive noise, vibration, and harshness transmission paths: road-input-related subframe vibration and engine-induced seat vibration. A standard cylindrical actuator was installed below the subframe of a passenger vehicle and tested on a rough road at 10, 20, and 30 km/h. Vehicle speed was used as the operating-condition feedback variable for current selection, while additional fixed-current measurements were conducted to characterize the current-dependent response. Cabin sound pressure was measured simultaneously. A compact actuator with a lightweight resin housing was also developed for the seat application; engine speed was used as the feedback variable, and the current was selected with reference to the second-order engine excitation. The natural frequencies of both actuators increased with current, although the compact actuator had a smaller tuning range. The actuator-installed conditions produced local, current-dependent reductions in subframe and seat vibration spectra. Changes in cabin sound pressure were smaller, frequency-dependent, and not uniform. The results demonstrate the feasibility of the operating-condition-based tuning of MRE dynamic absorbers for local automotive vibration paths, while also identifying limitations associated with passive installation effects, magnetic-circuit efficiency, packaging, and multi-path cabin acoustics.

Keywords: magnetorheological elastomer; semi-active vibration control; tunable dynamic vibration absorber; automotive subframe; seat vibration; road noise; structure-borne vibration; automotive NVH

Check for updates

Academic Editors: Tongfei Tian, Yingdan Liu, Shou-Hu Xuan and Yuhiro Iwamoto

Received: 2 July 2026
Revised: 8 August 2026
Accepted: 10 August 2026
Published: 13 August 2026

Copyright: © 2026 by the authors. Licensee MDPI, Basel, Switzerland. This article is an open access article distributed under the terms and conditions of the Creative Commons Attribution (CC BY) license.

1. Introduction

Automotive noise, vibration, and harshness (NVH) performance is becoming increasingly important as vehicles become increasingly electrified and lightweight and are equipped with advanced automated-driving functions [1–3]. In internal-combustion vehicles, powertrain noise can mask other vibration and noise sources. As this masking decreases, tire/road excitation, structure-borne road noise, and vibration transmitted through the seat become more perceptible. These trends increase the need for compact countermeasures that can adapt to changes in vehicle speed, engine speed, road surface, and structural operating condition.

Passive damping treatments, acoustic insulation, and tuned dynamic vibration absorbers remain attractive because of their robustness and simple implementation. However,

a conventional absorber is effective mainly around the frequency determined by its fixed mass, stiffness, and damping. Fully active systems can adapt to changing excitation by generating control forces or secondary sound fields [4–6] but generally require greater actuator authority, control hardware, and continuous power. Semi-active control provides an intermediate approach in which the device changes its mechanical properties without continuously generating a large counterforce. Frequency-tunable dynamic absorbers are, therefore, suitable for automotive applications in which the dominant excitation changes with the operating condition [7,8].

MREs are composite materials in which magnetic particles are dispersed in an elastomeric matrix. Their apparent stiffness changes when a magnetic field is applied [9–11]. When an MRE supports the movable mass of a dynamic absorber, the absorber's natural frequency can be varied by changing the magnetic field, typically through the current supplied to a coil. The device can consequently be tuned toward a target vibration component while retaining the basic mechanical simplicity of a passive absorber. Recent studies have further advanced MRE-based vibration isolation through dynamic modeling and control strategies, radial-chain structures with tunable stiffness and damping, and semi-active shear-mode absorber designs [12–14].

The authors previously developed MRE-based dynamic absorbers for broadband vibration reduction and automotive engine vibration applications [15–17]. In the broadband design, the coil served both as the magnetic-field generator and as the movable mass, reducing the number of separate components [16]. A later elliptical MRE design was applied to an automotive torque rod and reduced horizontal and vertical engine-induced vibration by selecting the current according to the excitation condition [17]. These studies established the current-dependent frequency-tuning principle and the operating-condition-based current-selection procedure used in the present work.

The applicability of this concept to other automotive NVH paths has not been sufficiently examined. Road excitation is transmitted through the tire, knuckle, suspension, and subframe before reaching the vehicle body, whereas seat vibration is transmitted through the body and seat-rail connections to the occupant. These paths differ from the previously investigated torque-rod path in terms of excitation level, frequency content, effective modal mass, available installation space, and practical packaging constraints. In addition, reducing a local subframe response does not necessarily produce an equivalent reduction in cabin sound pressure because cabin road noise is governed by multiple structural and airborne paths.

The objective of this study is to evaluate whether the existing MRE-based frequency-tunable absorber can be adapted to local subframe and seat vibration. A standard cylindrical actuator is installed on an automotive subframe and evaluated under rough-road driving, while a compact actuator is developed for a seat structure and evaluated under engine-induced excitation. In both applications, the operating condition is measured and used as a feedback variable for current selection. Fixed-current measurements are also presented to establish the tuning characteristics and to distinguish the zero-current passive response from the additional effect of magnetic-field-induced stiffness variation.

The principal contributions of this study are as follows:

1. The operating-condition-based semi-active tuning concept is applied to road-input-related subframe vibration using vehicle speed as the current-selection variable.
2. Subframe acceleration and cabin sound pressure are measured simultaneously to examine the limited and frequency-dependent acoustic influence of local structural vibration control.
3. A lightweight compact MRE actuator is developed for a seat structure and controlled with respect to engine speed and the corresponding second-order excitation frequency.

4. Fixed-current characterization is used to separate the passive effect of actuator installation from current-dependent frequency tuning and to compare the standard and compact actuator configurations.
5. The practical limitations of local modal control, ground clearance, magnetic-circuit efficiency, packaging, and multi-path NVH transmission are identified.

2. Materials and Methods

2.1. Principle of the MRE-Based Semi-Active Dynamic Absorber

The actuator is based on the principle of a dynamic vibration absorber. A secondary mass produces an inertial force that opposes the motion of a primary structure when the absorber natural frequency is close to the dominant excitation or structural-response frequency [18,19]. A passive absorber has fixed mechanical properties and, therefore, a limited effective frequency range. In the present device, the movable mass is supported by MRE elements whose apparent stiffness varies with the magnetic field, which allows the absorber frequency to be changed by the applied current.

The proposed actuator is classified as semi-active because the current modifies the absorber stiffness and natural frequency rather than commanding a large force proportional to the measured vibration. The magnetic field changes the dynamic characteristics of the attached secondary system, while the vibration-reduction force is generated by the relative motion of the movable mass. This operating principle differs from that of a conventional magnetorheological damper, in which a clipped-control law is commonly used to regulate damping force.

Figure 1 presents a local two-degree-of-freedom equivalent model adapted from the authors' previous work [16]. The parameters m_1, k_1, c_1, and x_1 denote the effective mass, stiffness, damping, and displacement of the local primary structure at the actuator attachment point, respectively; m_2, k_2, c_2, and x_2 denote the corresponding absorber parameters. The harmonic term $F_0 \cos \omega t$ represents an equivalent generalized force acting on the local structural mode. It does not imply that the vehicle tests were performed by directly applying a harmonic force. In the subframe test, this equivalent force represents road input transmitted through the tire, knuckle, and suspension; in the seat test, it represents engine-induced vibration transmitted through the vehicle body and seat rail.

$$m_1 \ddot{x}_1 + (c_1 + c_2)\dot{x}_1 + (k_1 + k_2)x_1 - c_2\dot{x}_2 - k_2x_2 = F_0 \cos\omega t, \quad (1)$$

$$m_2 \ddot{x}_2 + c_2\dot{x}_2 + k_2x_2 - c_2\dot{x}_1 - k_2x_1 = 0. \quad (2)$$

The natural angular frequency of the absorber is given by Equation (3).

$$\omega_0 = \sqrt{k_2/m_2}. \quad (3)$$

Because k_2 depends on the magnetic field acting on the MRE, the absorber natural frequency can be adjusted through the coil current. The current is selected so that the absorber frequency approaches the dominant local vibration component associated with the measured operating condition.

The coil performs two functions: it generates the magnetic field and acts as the movable mass. Integrating these functions eliminates a separate field coil or added tuning mass and reduces the number of independently assembled components. The arrangement also allows the magnetic flux to pass through the MRE supports and the surrounding ferromagnetic path while the coil moves relative to the housing.

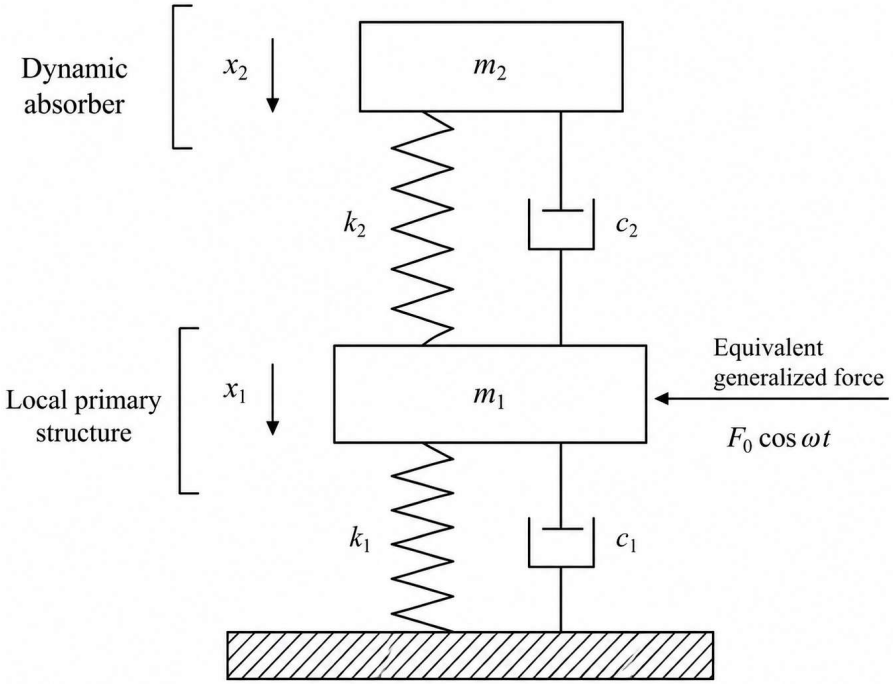


Figure 1. Local equivalent model of the MRE-based semi-active dynamic vibration absorber, adapted from Ref. [16]. The harmonic term represents the equivalent generalized force acting on the local target mode.

2.2. Fabrication of the Magnetorheological Elastomer

The MRE was fabricated by dispersing carbonyl iron powder (Carbonyl Fe OM, Fukuda Metal Foil & Powder Co., Ltd., Kyoto, Japan) in a silicone-rubber matrix (X-32-2428-4, Shin-Etsu Chemical Co., Ltd., Tokyo, Japan). RTV thinner (Shin-Etsu Chemical Co., Ltd., Tokyo, Japan) was added to adjust the viscosity during mixing, and a curing agent (X-32-2428-4, Shin-Etsu Chemical Co., Ltd., Tokyo, Japan) was added immediately before molding. The composition is summarized in Table 1; the median particle diameter of the iron powder was approximately 4.4 μm.

Table 1. Composition of the magnetorheological elastomer.

Material	Mass [g]
Silicone rubber	4.44
Iron powder	36.96
Thinner	3.00
Curing agent	0.45

The constituents were weighed, mixed, and degassed using a planetary centrifugal mixer (AR-100, THINKY Corporation, Tokyo, Japan). The mixture was poured into the actuator molding region after a silicone primer (Primer S, Shin-Etsu Chemical Co., Ltd., Tokyo, Japan) had been applied to the adjoining metallic surfaces to improve adhesion.

The MRE was cured at room temperature for 24 h while a magnetic field was applied. This process promoted particle alignment along the magnetic-field direction and preserved an anisotropic chain-like structure after curing. During actuator operation, the applied magnetic field changes the apparent stiffness of this particle-reinforced elastomer.

The same material formulation was used for the standard and compact actuator concepts. Differences in their tuning ranges, therefore, arise primarily from the movable mass, geometry, and magnetic-flux path rather than from a change in the MRE composition.

2.3. Configuration of the MRE Actuator

Figure 2 shows the standard cylindrical actuator used for the subframe application. The actuator comprises an aluminum outer housing, a steel inner housing and core, a movable copper coil, and upper and lower MRE supports. The basic configuration follows the previously developed frequency-tunable absorber [16]. Current supplied to the coil generates a magnetic field that passes through the steel components and MRE supports, changing the apparent MRE stiffness and the natural frequency of the movable coil.

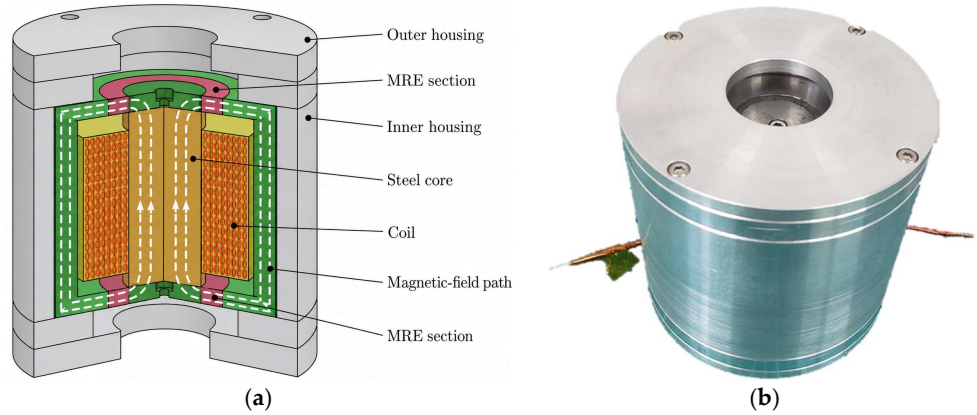


Figure 2. Standard cylindrical MRE actuator used for the subframe application: (**a**) cross-sectional schematic and (**b**) fabricated actuator. The green regions in panel (**a**) indicate the MRE supports schematically and do not represent a different MRE formulation from that reported in Ref. [16].

Using the coil as both the field generator and movable mass reduces the component count because a separate tuning mass and a separate stationary excitation coil are unnecessary. The integrated configuration also concentrates the magnetic circuit around the MRE supports and permits the movable element to respond along the principal vibration-control direction.

The coil was wound with 1.3 mm diameter copper wire and comprised approximately 330 turns. Flexible lead wires were installed with sufficient slack to avoid mechanically constraining the coil motion. The movable coil mass was 0.50 kg.

The principal dimensions and masses of the standard actuator are listed in Table 2. These values define the actuator used in the subframe experiment; the separately developed compact seat actuator is described in Section 2.6.

Table 2. Dimensions and masses of the main components of the MRE actuator.

Component	Dimensions [mm]	Mass [kg]	Material
Outer housing	φ94.0 × 63.0	0.56	Aluminum alloy
Inner housing	φ78.0 × 53.0	1.06	Steel
MRE support	φ31.5 × φ25.5 × 5.0	0.010	Silicone rubber/iron powder
Steel core	φ25.5 × 51.0	0.20	Steel
Coil	φ58.0 × φ25.5 × 36.0	0.50	Copper wire

2.4. Operating-Condition-Based Semi-Active Current Control

The control objective is to change the absorber natural frequency by adjusting the coil current. Unlike clipped control for an MR damper, the present system does not command a target damping force. Instead, a measured operating condition is used as a feedback variable, and the current is selected from an experimentally established relationship between current and actuator natural frequency.

Before the vehicle tests, hammer-impact measurements were performed at discrete currents to determine the current–natural frequency relationship for each actuator. The standard cylindrical actuator was characterized over 0–4 A using 0.5 A increments, whereas the compact actuator was characterized over 0–3 A using 1 A increments in the available calibration dataset. Separate calibration relationships were required because the two actuators differed in terms of movable mass, housing material, magnetic circuit, and attainable tuning range.

For the subframe application, vehicle speed was measured and used as the operating-condition feedback variable. The current-selection map related vehicle speed and the dominant road-input-related subframe response to the calibrated actuator frequency. During each constant-speed spectral record, the selected current remained constant because the operating condition was held constant.

For the seat application, engine speed N, expressed in RPM, was measured and used as the feedback variable. For the inline-four four-stroke engine, the principal second-order excitation frequency was calculated as $f_2\ (\mathrm{Hz}) = 2N/60 = N/30$. The compact-actuator current was selected from its calibration relationship so that its natural frequency approached the second-order excitation associated with the measured engine speed.

The current command was restricted to the allowable current range of the corresponding coil and power supply. Because the calibration relationship is nonlinear, the control procedure used the experimentally determined map rather than assuming a single linear current–frequency equation over the entire range. The underlying tuning and current-selection concept follows Ref. [16].

The 0 A condition is distinct from the condition without the actuator. At 0 A, the actuator remains mechanically attached and functions as a passive absorber with its zero-field stiffness, added mass, attachment stiffness, and inherent damping. The difference between the without-actuator and 0 A conditions, therefore, represents the passive installation effect, while differences among the 0 A and nonzero-current conditions indicate the additional influence of magnetic-field-dependent tuning.

Fixed-current measurements were also conducted. These measurements were conducted to characterize the actuator dynamics, construct or verify the current-selection maps, and compare candidate current states at a fixed operating condition. They should not be interpreted as the complete time history of the operating-condition-based controller. When vehicle speed or engine speed was constant during an individual record, the selected current was correspondingly constant.

Table 3 summarizes the operating-condition variables, target frequency relations, calibration ranges, and fixed-current records reported for the two applications.

The present implementation focuses on operating-condition feedback rather than direct closed-loop minimization of an acceleration error. Consequently, its performance depends on the calibration map, the repeatability of the excitation path, and the relationship between the measured operating variable and the dominant local vibration frequency.

Table 3. Summary of operating-condition-based current selection and fixed-current characterization.

Application	Feedback Variable	Current-Selection Basis	Fixed-Current Records Reported
Subframe	Vehicle speed	Standard-actuator calibration from 0 to 4 A at 0.5 A increments; current selected to approach the dominant local subframe component	3 A at 10, 20, and 30 km/h; 0 A, 1 A, 2 A, 3 A, and 4 A at 20 km/h
Seat	Engine speed, N [RPM]	Second-order target f_2 (Hz) $= N/30$; compact-actuator calibration from 0 to 3 A at 1 A increments	0 A, 2 A, and 3 A at 1500 RPM

2.5. Application to the Automotive Subframe System

The standard actuator was applied to the subframe to target a local structure-borne vibration path associated with road input. Road excitation is transmitted from the tire through the knuckle, suspension members, and subframe to the vehicle body. The actuator was not intended to suppress the rigid-body motion of the entire vehicle; it was intended to modify the local subframe response near the suspension-input path.

Figure 3 shows the experimental installation. The actuator was attached below the subframe, and a PCB Piezotronics 352C41 piezoelectric accelerometer (PCB Piezotronics, Inc., Depew, NY, USA) was mounted on the subframe adjacent to the actuator attachment point. The actuator axis and accelerometer measurement direction were aligned with the dominant local vibration direction.

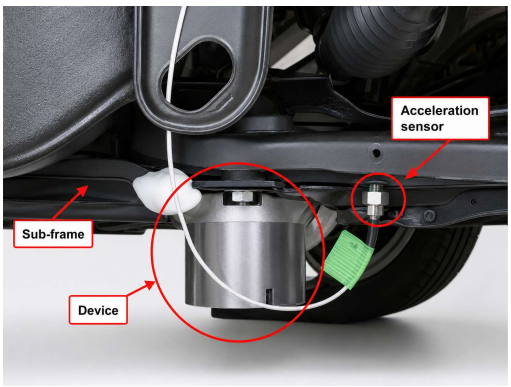


Figure 3. Experimental installation of the standard cylindrical MRE actuator and accelerometer on the automotive subframe.

A 2008 Nissan Bluebird Sylphy (Nissan Motor Co., Ltd., Yokohama, Japan) with a 2.0 L inline-four engine and continuously variable transmission was used. Tests were conducted on a controlled rough-road section at constant speeds of 10, 20, and 30 km/h, with the transmission in the drive range. The below-subframe installation locally reduced the available ground clearance; however, the actuator did not contact the road surface, including during passage over road irregularities, and no adverse influence on low-speed handling or stability was observed. This installation was used only for experimental validation and is not proposed as a production mounting configuration.

Subframe acceleration was measured using a PCB Piezotronics 352C41 accelerometer (sensitivity 1.02 mV/(m/s^2), measurement range ±4905 m/s^2, frequency range within ±5% from 1 to 9000 Hz, mass 2.8 g). Cabin sound pressure was measured using a PCB Piezotronics 130F20 microphone (PCB Piezotronics, Inc., Depew, NY, USA) positioned at the driver's ear height on the inboard side of the headrest. Both signals were acquired simultaneously

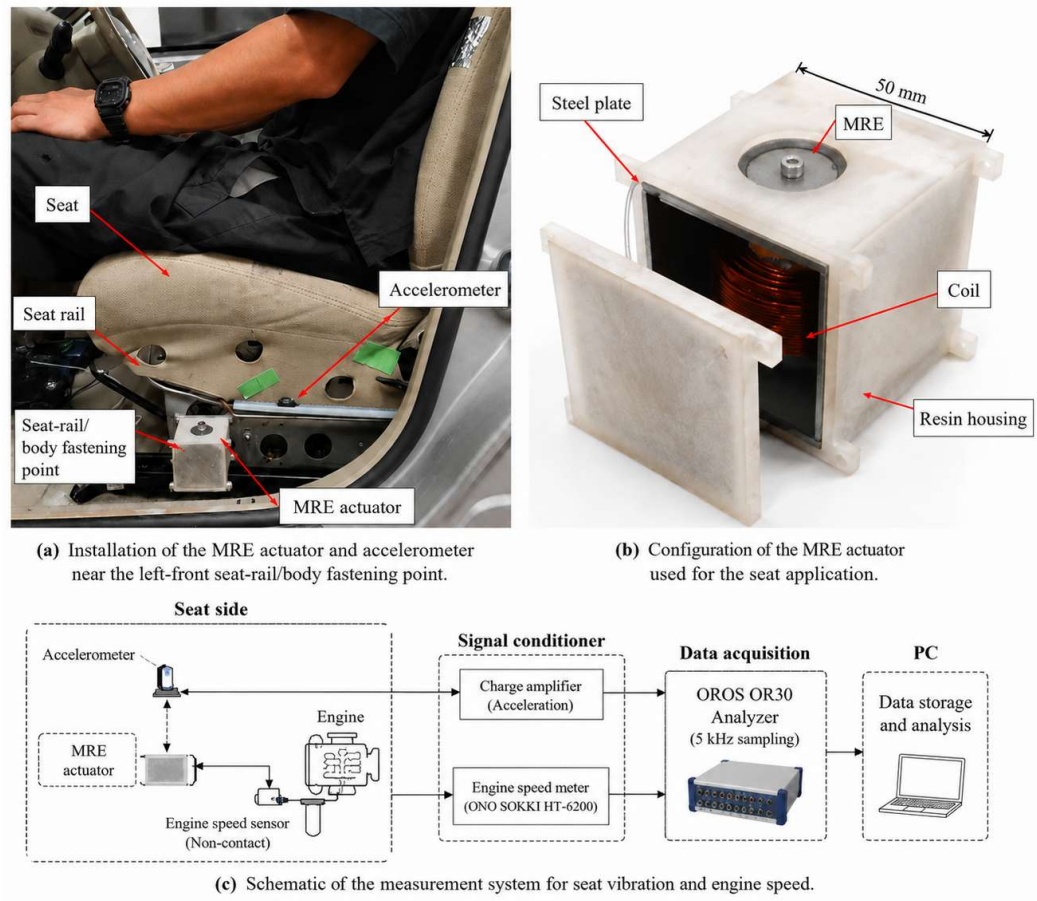
using a Keyence NR-500 data logger with an NR-CA04 sensor unit (KEYENCE Corporation, Osaka, Japan) at a sampling frequency of 100 kHz.

Vehicle speed was used for operating-condition-based current selection. The subframe spectra obtained without the actuator and with the selected current were compared, and additional fixed-current records at 20 km/h were used to examine current sensitivity and the passive 0 A condition. Cabin sound pressure was analyzed under the corresponding driving conditions to determine whether local subframe control produced a measurable, although not necessarily causal, change in the cabin acoustic response.

2.6. Application to the Automotive Seat System

The second application addressed vertical vibration transmitted through the seat structure. Compared with the engine-related vibration examined in the authors' previous MRE application [17] and the road-input subframe vibration considered in Section 2.5, the measured seat vibration level was relatively small, and the available installation space was more restricted. A separate compact and lightweight actuator was, therefore, developed for this application.

Figure 4 shows the seat installation, the compact actuator, and the measurement system. The compact device retained the same MRE-supported movable-coil principle as the standard actuator, but it used a rectangular resin housing to reduce mass and improve installation flexibility. The standard cylindrical actuator in Figure 2 and the compact seat actuator in Figure 4 are, therefore, different hardware implementations of the same frequency-tuning concept.



(a) Installation of the MRE actuator and accelerometer near the left-front seat-rail/body fastening point.

(b) Configuration of the MRE actuator used for the seat application.

(c) Schematic of the measurement system for seat vibration and engine speed.

Figure 4. Experimental setup for the automotive seat system: (**a**) installation of the MRE actuator and accelerometer near the left-front seat-rail/body fastening point; (**b**) MRE actuator configuration; and (**c**) measurement system for seat vibration and engine speed.

The compact housing measured approximately 50 mm across. Steel plates with a thickness of 5 mm were arranged inside the nonmagnetic resin housing to form a magnetic-flux path, and the movable coil mass was reduced to 0.20 kg. The housing was fabricated by three-dimensional printing. This design improved packaging and manufacturability, but the discontinuous steel-plate path was less magnetically efficient than the continuous metallic path of the cylindrical actuator.

The compact actuator was installed on the lower seat structure adjacent to the left-front seat-rail/body fastening point. The same vehicle was used with the transmission in neutral. Engine speed was increased from approximately 700 to 4500 RPM to allow the engine-induced excitation frequency to vary while excluding road input. Engine speed was measured in real time and used for current selection based on the corresponding second-order frequency.

Vertical acceleration was measured using a PCB Piezotronics 352C41 accelerometer mounted at the left-front fastening point between the seat rail and the vehicle body. The acceleration signal was acquired using an OROS OR30 analyzer (OROS Digital S.A.S., Montbonnot-Saint-Martin, France) at 5 kHz for 10 s and analyzed using a Hanning window. Engine speed was measured by positioning the IP-3000A sensing unit of an ONO SOKKI HT-6200 non-contact engine-speed meter (Ono Sokki Co., Ltd., Yokohama, Japan) near the engine ignition coil.

The operating-condition-based controller selected current from the compact-actuator calibration map. In addition, fixed-current records at 0, 2, and 3 A were obtained at 1500 RPM to compare candidate tuning states around the 50 Hz second-order engine component. The primary evaluation quantity was the vertical acceleration at the seat-rail/body fastening point; direct occupant comfort and subjective ride evaluation were outside the scope of this study.

2.7. Measurement and Evaluation Conditions

The measurement instruments and acquisition conditions are summarized in Table 4, while the principal vehicle and excitation conditions are summarized in Table 5. The subframe and cabin measurements were conducted simultaneously during constant-speed rough-road driving, whereas the seat measurement was conducted during a stationary engine-speed sweep. The two applications, therefore, used different operating-condition variables and different acquisition systems.

For the subframe application, the vehicle-speed signal determined the current-selection state. For the seat application, the measured engine speed was converted to the second-order excitation frequency and used to select the compact-actuator current. Because each reported spectrum corresponds to a time interval with a nominally constant operating condition, the current is identified by a discrete value in the figures even though the overall control strategy is based on the measured operating condition.

Acceleration levels in the subframe and seat results were calculated as $L_a = 20 \log_{10}(a/a_{\mathrm{ref}})$, where a is the acceleration amplitude at each frequency and $a_{\mathrm{ref}} = 1\ \mathrm{m/s^2}$. Accordingly, an acceleration amplitude of $1\ \mathrm{m/s^2}$ corresponds to 0 dB. The cabin sound-pressure spectra are presented as relative levels. The maximum level measured under the without-actuator condition over the three vehicle speeds was defined as 0 dB, and the same offset was applied to all spectra. No frequency weighting was applied. The subframe acceleration and cabin sound-pressure signals were transformed to frequency-domain spectra using the recorded road-test intervals. The seat result was evaluated by order-related frequency interpretation using the measured engine speed, with particular attention to the second-order component.

Table 4. Measurement instruments and acquisition conditions.

Analysis Setting	Sampling	Key Specification or Position	Instrument/Model	Measurement
Frequency-domain road-test analysis	100 kHz	1.02 mV/(m/s^2); ±4905 m/s^2; 1–9000 Hz (±5%); 2.8 g; adjacent to actuator	PCB Piezotronics 352C41	Subframe acceleration
Simultaneous with subframe acceleration	100 kHz	Driver-ear height, inboard side of headrest	PCB Piezotronics 130F20	Cabin sound pressure
10 s record; Hanning window	5 kHz	Vertical; left-front seat-rail/body fastening point	PCB Piezotronics 352C41	Seat acceleration
Second-order frequency calculated from engine speed	Recorded with seat test	Non-contact sensing near ignition coil	ONO SOKKI HT-6200 with IP-3000A	Engine speed
Frequency-domain and order-related interpretation	100 kHz; 5 kHz	Subframe/cabin; seat, respectively	Keyence NR-500 + NR-CA04; OROS OR30	Acquisition system

Table 5. Experimental conditions for the subframe and seat applications.

Item	Subframe Application	Seat Application
Test vehicle	Nissan Bluebird Sylphy	Nissan Bluebird Sylphy
Engine	2.0 L inline-four engine	2.0 L inline-four engine
Transmission	Continuously variable transmission	Continuously variable transmission
Test condition	Constant-speed rough-road test	Stationary engine-speed sweep
Vehicle speed	10, 20, and 30 km/h	0 km/h
Gear position	Drive range	Neutral
Engine speed	Approximately constant during each test	Approximately 700–4500 RPM
Main excitation source	Road input transmitted through suspension/subframe	Engine second-order excitation
Main evaluation target	Local subframe acceleration and cabin sound pressure	Vertical acceleration at seat-rail/body fastening point

Three reference states were distinguished throughout the analysis: without actuator, actuator installed at 0 A, and actuator installed at a nonzero current. This distinction prevents the passive effect of added mass and attachment from being attributed entirely to MRE tuning.

The reported comparisons assess local spectral changes under the tested conditions. They do not constitute a complete transfer-path isolation, whole-vehicle vibration evaluation, or occupant comfort assessment.

3. Results

3.1. Dynamic Characteristics of the MRE Actuator

The current-dependent natural frequencies of the two actuators were identified before the vehicle tests. Figure 5 presents the calibration data used for the current selection. Applied current is plotted on the horizontal axis because it is the controlled independent variable, and actuator natural frequency is plotted on the vertical axis.

For the standard cylindrical actuator used on the subframe, the natural frequency increased from approximately 25 Hz at 0 A to approximately 125 Hz at 4 A. Measurements were summarized at 0.5 A intervals. The monotonic increase confirms that the magnetic field increased the effective stiffness of the MRE supports over the tested range.

For the compact seat actuator, the natural frequency increased from approximately 50 Hz at 0 A to approximately 63 Hz at 3 A. The available calibration data were summarized at 1 A intervals. The smaller shift does not indicate a different operating principle; it reflects the lower movable mass, resin housing, and less continuous magnetic-flux path of the compact design.

The current–frequency relationship was nonlinear, particularly for the standard actuator. The calibration points were, therefore, used directly for current mapping rather than being represented by a single linear equation. This approach also avoids introducing undefined fitting coefficients and permits separate calibration of the two actuator configurations.

Both devices retained measurable current-dependent tunability. The standard actuator provided the broader range required for subframe vibration components, whereas the compact actuator traded tuning range for reduced mass and improved installation flexibility.

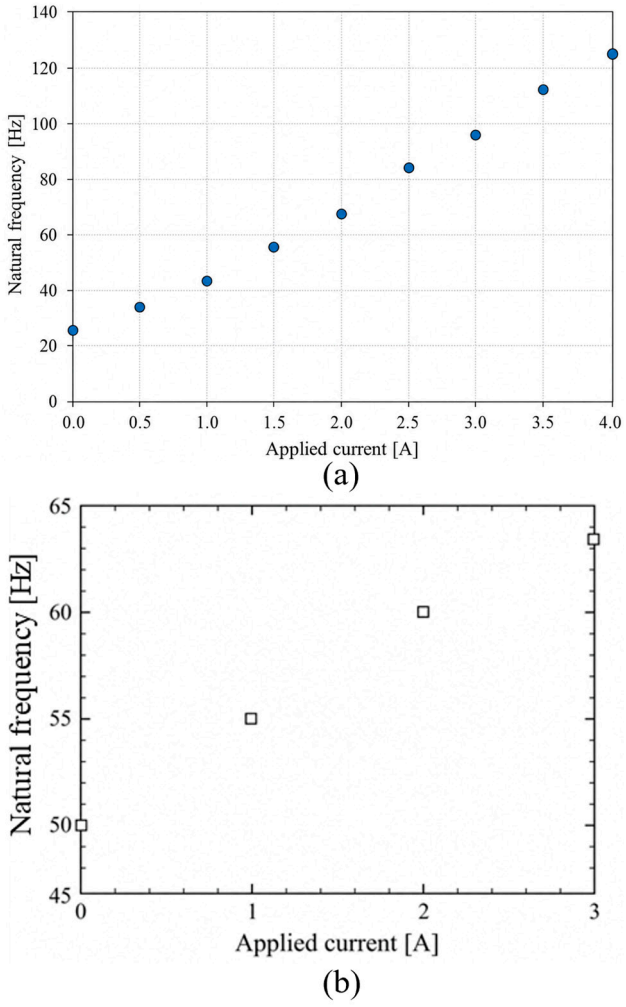


Figure 5. Current-dependent natural frequencies of the MRE actuators: (**a**) standard cylindrical actuator used for the subframe application, measured from 0 to 4 A at 0.5 A increments; and (**b**) compact seat actuator, summarized from 0 to 3 A at 1 A increments.

3.2. Subframe Vibration Reduction

Figure 6 compares the subframe acceleration spectra obtained without the actuator and with the actuator at 3 A during rough-road driving at 10, 20, and 30 km/h. The 3 A records

are representative constant-current intervals selected under the corresponding operating conditions. Road input produced multiple broadband and narrowband components because the measured response included the combined dynamics of the tire, suspension, subframe, and vehicle body.

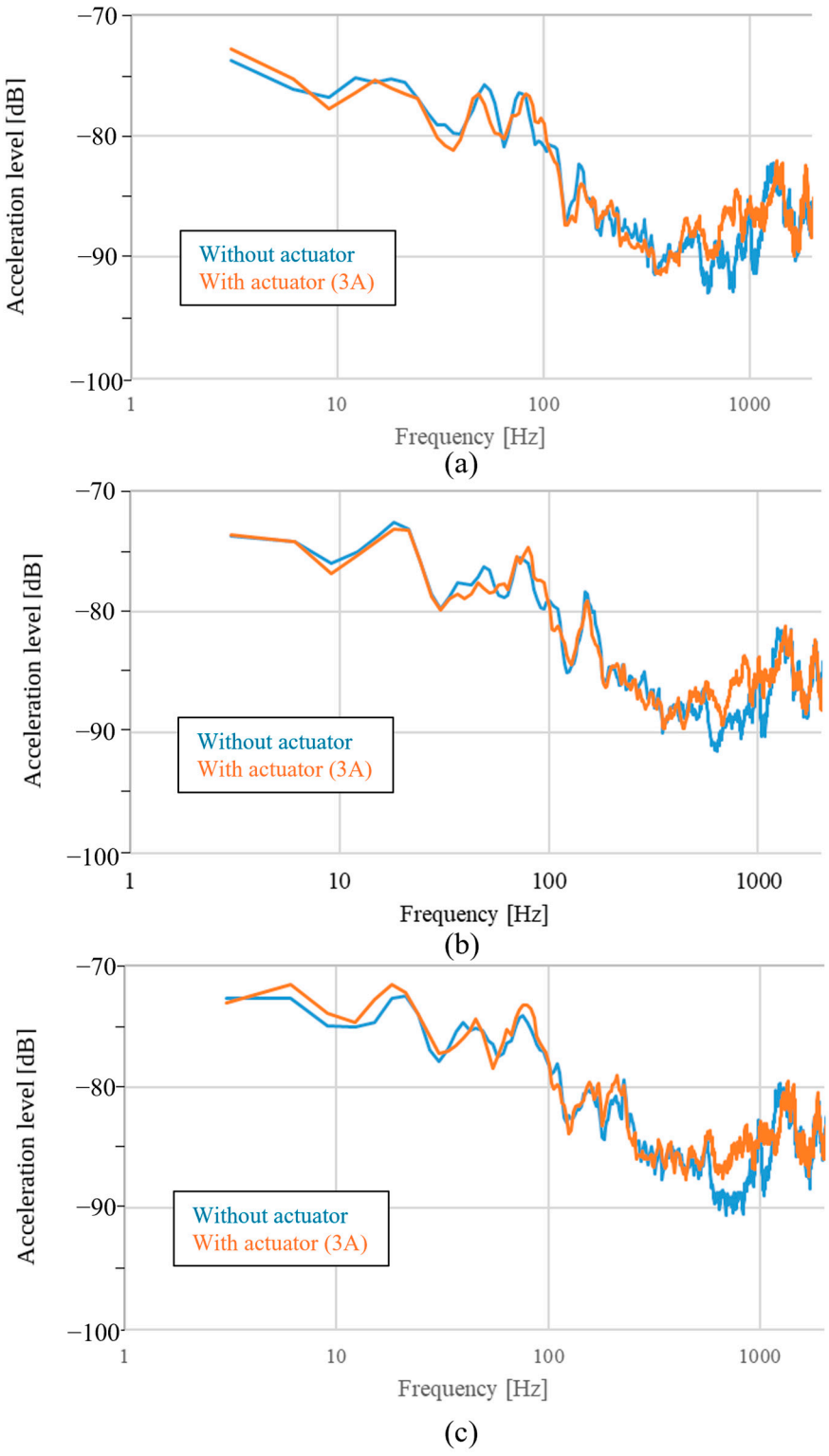


Figure 6. Subframe acceleration spectra with and without the MRE actuator during rough-road driving: (**a**) 10 km/h, (**b**) 20 km/h, and (**c**) 30 km/h. The actuator current was 3 A. The acceleration level is referenced to 1 m/s^2; 0 dB corresponds to 1 m/s^2 and lies above the plotted range.

At all three speeds, the actuator-installed condition differed from the without-actuator condition in selected frequency regions. Local decreases were observed near several dominant components and in portions of the higher-frequency range, while other regions changed little or occasionally increased. The result is, therefore, not a uniform broadband attenuation. It represents the combined effect of passive installation and the 3 A tuning state.

The 20 km/h result showed particularly clear current-dependent differences and was selected for additional fixed-current characterization. The without-actuator and 3 A spectra shown in Figure 7 are based on the same measurement datasets as those shown in Figure 6b.

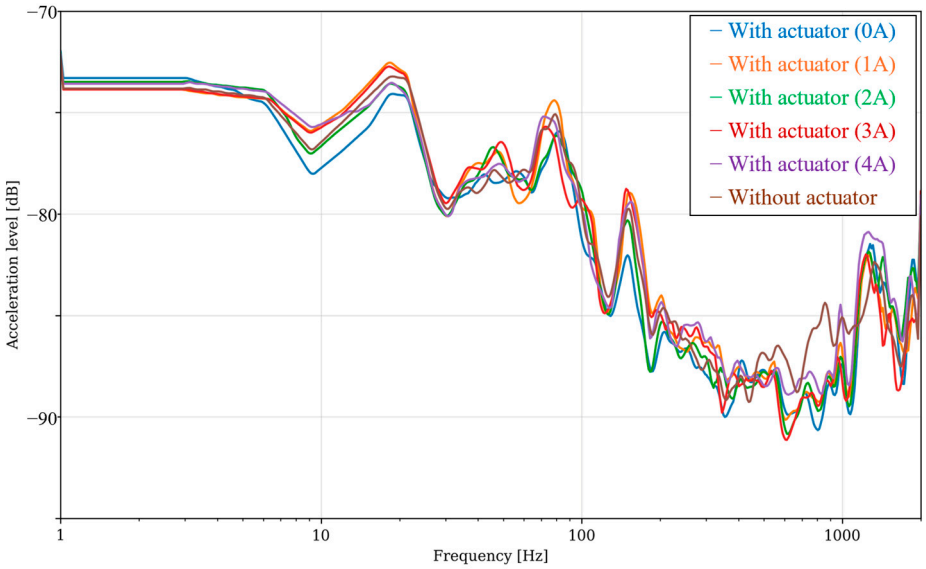


Figure 7. Fixed-current characterization of the subframe acceleration spectra during rough-road driving at 20 km/h. The without-actuator condition is compared with actuator-installed states at 0, 1, 2, 3, and 4 A. The acceleration level is referenced to 1 m/s^2; 0 dB corresponds to 1 m/s^2 and lies above the plotted range.

Figure 7 compares the without-actuator condition with fixed-current states of 0, 1, 2, 3, and 4 A at 20 km/h. The difference between the without-actuator and 0 A curves demonstrates that installing the device changes the local structural response even without a magnetic field. Differences among the installed states show that the response is further modified as MRE stiffness and actuator natural frequency change with current.

No single current produced the lowest acceleration across the entire frequency range. This is expected for a tunable dynamic absorber: the most effective current depends on the target vibration component rather than simply increasing with current magnitude. The fixed-current comparison, therefore, provides the experimental basis for the vehicle-speed-based current-selection map.

3.3. Influence on Cabin Sound Pressure

Figure 8 compares cabin sound pressure near the driver's ear position without the actuator and with the subframe actuator at 3 A during the same 10, 20, and 30 km/h rough-road conditions. The purpose of this comparison was to examine whether a measurable cabin-acoustic change accompanied the local subframe response change.

The actuator-installed condition produced local decreases in several frequency regions, but the differences were smaller and less systematic than those observed in the subframe acceleration. Other regions showed little change or condition-dependent increases. These spectra, therefore, do not demonstrate uniform cabin road-noise reduction.

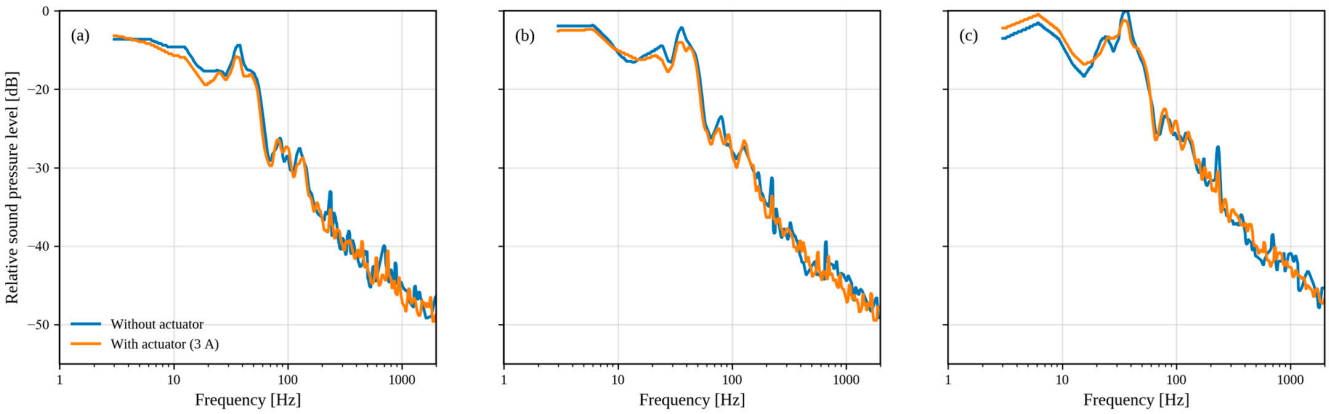


Figure 8. Relative cabin sound-pressure spectra with and without the subframe MRE actuator during rough-road driving: (**a**) 10 km/h, (**b**) 20 km/h, and (**c**) 30 km/h. The actuator current was 3 A. The maximum level measured under the without-actuator condition over the three vehicle speeds was defined as 0 dB, and the same offset was applied to all spectra. No frequency weighting was applied.

The complex response is consistent with the multi-path nature of cabin road noise. Tire/road excitation reaches the cabin through the suspension, subframe, body, airborne paths, and interior acoustic modes. A local change at the subframe measurement point is, consequently, not expected to produce a proportional change at the driver's ear over the full spectrum.

The results provide preliminary evidence that changing the local subframe response can influence part of the cabin sound-pressure spectrum. A causal assessment would require transfer-path analysis and repeated measurements focused on the frequency bands with strong subframe-to-cabin transmission.

3.4. Seat Vibration Response

Figure 9 presents the fixed-current characterization of the seat vibration at an engine speed of 1500 RPM. Figure 9a shows the overall 0–200 Hz spectrum, and Figure 9b enlarges the region around the 50 Hz second-order component of the inline-four four-stroke engine.

The without-actuator and 0 A curves differ, which confirms a passive installation effect associated with the compact absorber mass, attachment, zero-field stiffness, and damping. The 2 and 3 A curves show additional current-dependent changes, consistent with the compact-actuator calibration in Figure 5b.

Around the second-order component, the relative levels and spectral shapes depend on current. The 2 A condition produces a pronounced local reduction near 50 Hz compared with the 0 A state, while the neighboring peaks respond differently. These results illustrate why the engine-speed-based controller must select current according to the target order rather than current magnitude alone.

The compact actuator did not reduce the entire spectrum. Its effect was local and limited by the approximately 50–63 Hz tuning range of the present magnetic circuit. The result should, therefore, be interpreted as a feasibility demonstration of current-dependent modification of the seat-rail response, not as validation of broadband ride-comfort improvement.

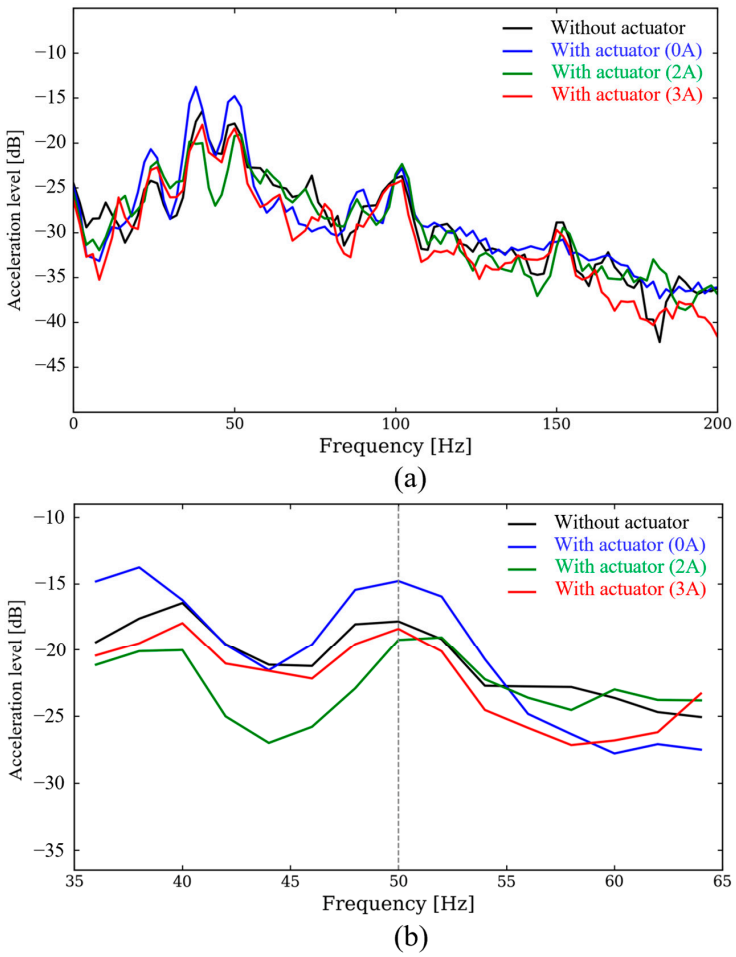


Figure 9. Fixed-current characterization of seat vibration at 1500 RPM: (**a**) overall spectrum from 0 to 200 Hz and (**b**) enlarged view around the 50 Hz engine second-order component. The without-actuator condition is compared with compact-actuator states at 0, 2, and 3 A. The acceleration level is referenced to 1 m/s^2; 0 dB corresponds to 1 m/s^2 and lies above the plotted range.

4. Discussion

4.1. Effectiveness of Frequency-Tunable Semi-Active Control

The experiments confirm the central actuator principle: increasing current increases MRE support stiffness and shifts the natural frequency of the movable coil. The standard and compact devices, therefore, provide controllable mechanical states without generating a continuously commanded counterforce. The appropriate description is a frequency-tunable semi-active dynamic absorber, rather than an MR damper controlled by a clipped-force law.

Operating-condition feedback was implemented differently for the two applications. Vehicle speed was used for the subframe current-selection map, while engine speed and the corresponding second-order frequency were used for the seat map. Fixed-current spectra were retained because they reveal the physical basis of the map and distinguish passive installation from magnetic-field-dependent tuning. During a constant-speed or constant-engine-speed record, a constant current is fully consistent with an operating-condition-based controller.

The movable mass of the standard actuator was 0.50 kg, which is small compared with the total vehicle mass. This comparison is not the relevant criterion, however, because the actuator did not attempt to control whole-vehicle rigid-body motion. A tuned absorber acts on the effective modal mass and mobility of the local subframe mode at its attachment point.

Placement near the suspension-input path and tuning near a dominant local component allow a comparatively small movable mass to modify the measured response.

The current-dependent differences were frequency selective, as expected. Higher current did not always produce lower vibration because increasing current shifts the absorber frequency rather than monotonically increasing a broadband damping force. The effectiveness of the method, therefore, depends on calibration accuracy, target frequency identification, attachment-point mobility, and the damping of both the target structure and absorber.

The present results support the feasibility of the current-selection concept but do not quantify transient tracking performance during rapid changes in speed. Future controller development should improve map resolution, switching logic, response time, and robustness to changes in road surface, temperature, load, and structural condition.

4.2. Relationship Between Subframe Vibration and Cabin Sound Pressure

The subframe is one of the principal local transmission components between the suspension input and the vehicle body. The measured acceleration reductions, therefore, show that the MRE actuator can modify a road-input-related structure-borne path near the knuckle and suspension connection.

The cabin sound-pressure changes were smaller than the local structural changes. This does not contradict the subframe result because the cabin measurement combines multiple structural and airborne paths. The present evidence supports an influence on selected acoustic components but not a complete causal demonstration of cabin road-noise reduction.

A stronger assessment would require repeated controlled runs, coherence or operational transfer-path analysis, and simultaneous measurements at additional suspension, body, and cabin locations. These methods would identify the frequency bands in which subframe mobility contributes most strongly to the driver-ear response and would support optimized actuator placement and current selection.

The acoustic conclusion is, therefore, deliberately limited: local subframe tuning produced measurable, frequency-dependent cabin spectral changes under the tested conditions, while the overall cabin benefit remains to be established.

4.3. Applicability to Occupant-Transmitted Seat Vibration

The seat application demonstrates that the same physical principle can be packaged for a smaller and lower-level vibration path. The rectangular resin housing and 0.20 kg movable coil reduced mass and improved installability around the seat rail, where the standard cylindrical device could not be accommodated readily.

The reduced tuning range of the compact device is attributable to its magnetic circuit. The resin housing does not guide magnetic flux, and the internal steel plates provide a less continuous path than the cylindrical steel housing. The resulting lower flux efficiency limits the field-induced stiffness change. This trade-off between packaging and magnetic performance is a central design issue for practical seat integration.

At 1500 RPM, current-dependent changes occurred around the 50 Hz second-order component. Because the accelerometer was mounted at the seat-rail/body fastening point, the result represents a local transmitted vibration response rather than the acceleration of the occupied seat cushion or a direct comfort metric. No claim of subjective comfort improvement is made.

Future work should examine the repeatability of the current-dependent vibration reduction and further optimize the actuator structure and attachment condition.

4.4. Comparison with Previous Engine Vibration Applications

The present work extends the authors' previous broadband and engine-torque-rod studies [15–17]. The actuator physics remains the same: magnetic-field-dependent MRE stiffness is used to tune the natural frequency of an attached movable mass. The contribution of the present study is the engineering adaptation of this principle to two additional NVH paths with substantially different input mechanisms and packaging constraints.

The subframe application addresses road input transmitted through the suspension and demonstrates local vibration modification at a structural path related to cabin road noise. The seat application addresses engine-induced vibration at a body-to-seat connection and introduces a separate compact actuator. These applications show that the actuator configuration and current map must be tailored to the target path rather than transferred unchanged.

The standard cylindrical actuator offers a broad tuning range and is suitable for locations with greater available space and stronger structural input. The compact actuator offers lower mass and improved installation flexibility but a narrower tuning range. This comparison provides design guidance for distributed semi-active devices in future vehicle structures.

This study does not propose a new MRE constitutive mechanism or a new general control theory. Its novelty lies in demonstrating operating-condition-based adaptation and local experimental feasibility across distinct automotive NVH transmission paths.

4.5. Limitations and Future Work

Several limitations should be recognized. First, one vehicle, one principal rough-road surface, and a limited set of speeds and engine conditions were evaluated. Run-to-run variability and statistical confidence were not quantified comprehensively.

Second, the current-selection maps were based on discrete calibration and characterization data. Although vehicle speed and engine speed were used as feedback variables, transient switching performance, hysteresis, temperature dependence, and robustness to changing road and load conditions were not evaluated.

Third, the temporary subframe installation reduced local ground clearance. No road contact or adverse handling effect occurred in the low-speed tests, including passage over irregularities, but practical implementation would require packaging within the original vehicle or subframe envelope while maintaining the specified minimum ground clearance.

Fourth, the compact actuator had a limited tuning range because of magnetic-circuit inefficiency. Magnetic design, thermal behavior, coil power consumption, durability, and long-term MRE stability require further evaluation for both actuator types.

Finally, the measurements primarily describe local frequency-domain acceleration and sound-pressure spectra. Transfer-path analysis, repeated tests, statistical uncertainty, psychoacoustic metrics, weighted whole-body vibration indices, and subjective evaluation are necessary before claiming production-level road-noise or ride-comfort improvement.

5. Conclusions

This study evaluated the extension of an MRE-based frequency-tunable dynamic absorber to local automotive subframe and seat vibration. The main findings are summarized below.

1. The natural frequency of the standard cylindrical actuator increased from approximately 25 to 125 Hz over 0–4 A, while that of the compact seat actuator increased from approximately 50 to 63 Hz over 0–3 A. The nonlinear calibration data support current-map-based tuning rather than a single linear approximation.

2. Vehicle speed and engine speed were used as operating-condition feedback variables for the subframe and seat applications, respectively. Fixed-current measurements clarified the current-dependent response and separated the passive 0 A state from the effect of magnetic-field-induced tuning.
3. The subframe actuator produced local, frequency-dependent changes and reductions in acceleration during rough-road driving at 10, 20, and 30 km/h. Its 0.50 kg movable mass acted on the local effective modal response near the suspension-input path, not on the total vehicle mass.
4. Cabin sound-pressure changes were measurable but smaller and less uniform than the subframe changes. The results indicate a possible influence on the selected structure-borne components but do not establish complete cabin road-noise reduction.
5. The compact seat actuator produced current-dependent changes around the 50 Hz second-order engine component at 1500 RPM. The result supports feasibility for local seat-rail vibration control, while the limited tuning range and absence of occupant-based evaluation preclude a claim of broadband comfort improvement.

Practical application requires improved calibration-map resolution, transient controller evaluation, magnetic and thermal optimization, packaging within the vehicle envelope, repeated testing, transfer-path analysis, durability assessment, and objective and subjective NVH evaluation.

6. Patents

The MRE-based vibration control device described in this study is related to Japanese Patent No. 7101410, "Active Vibration Control Device," by Takumi Naito, Osamu Terashima, Hiroshi Endo, and Kenichi Sugioka.

Author Contributions: All authors contributed to the methodology. Y.S., Y.Y., Y.K. and R.N.A. contributed to the investigation, data processing, formal analysis, visualization, discussion, and original draft preparation. O.T. contributed to the conceptualization, supervision, project administration, funding acquisition, and manuscript review and editing. All authors have read and agreed to the published version of the manuscript.

Funding: This research was funded by JSPS KAKENHI Grant Number 22H01426, the Mazak Foundation, and the Kansai Research Foundation for Technology Promotion. The article processing charge was waived by the publisher.

Institutional Review Board Statement: Not applicable.

Informed Consent Statement: Not applicable.

Data Availability Statement: The data presented in this study are available on request from the corresponding author. The data are not publicly available because they include experimental data obtained from vehicle tests and are part of ongoing research.

Acknowledgments: The authors would like to express their sincere gratitude to Takumi Naito, Ryo Kiyotaki, and Zhe Li for their contributions to the development of the MRE-based vibration absorbers and related experimental investigations.

Conflicts of Interest: The authors declare no conflicts of interest. The funders had no role in the design of the study; in the collection, analyses, or interpretation of data; in the writing of the manuscript; or in the decision to publish the results. The article processing charge waiver had no influence on the study design, results, interpretation, or publication decision.

References

1. Haider, M. Electrifying times: Restructuring and decision-making in an automobile concern in the 21st century—The case of BMW Group. *Hung. Geogr. Bull.* **2020**, *69*, 119–135. [CrossRef]
2. Shima, T.; Nagasaki, T.; Kuriyama, A.; Yoshimura, K.; Sobue, T. Fundamental technologies driving the evolution of autonomous driving. *Hitachi Rev.* **2016**, *65*, 56–62.
3. Smart, A.; Stetson, C.; Jesudesan, K. Autonomous vehicle safety assessment with fully quantified ODDs. *SAE Int. J. Adv. Curr. Pract. Mobil.* **2022**, *4*, 270–277. [CrossRef]
4. Hansen, C.; Snyder, S.; Qiu, X.; Brooks, L.; Moreau, D. *Active Control of Noise and Vibration*, 2nd ed.; CRC Press: Boca Raton, FL, USA, 2012; pp. 1–13.
5. Sano, H.; Inoue, T.; Takahashi, A.; Yamashita, T.; Nakamura, M.; Terai, K.; Nakamura, Y. Development of active control system for low frequency road noise: Solutions for practical use and system configuration. *Acoust. Sci. Technol.* **2001**, *22*, 378–379. [CrossRef]
6. Sakamoto, K.; Inoue, T. Development of feedback-based active road noise control technology for noise in multiple narrow-frequency bands and integration with booming noise active noise control system. *SAE Int. J. Passeng. Cars Mech. Syst.* **2015**, *8*, 1–7. [CrossRef]
7. Turco, E.; Gardonio, P. Sweeping shunted electro-magnetic tuneable vibration absorber: Design and implementation. *J. Sound Vib.* **2017**, *407*, 82–105. [CrossRef]
8. Gardonio, P.; Casagrande, D. Shunted piezoelectric patch vibration absorber on two-dimensional thin structures: Tuning considerations. *J. Sound Vib.* **2017**, *395*, 26–47. [CrossRef]
9. Han, Y.; Hong, W.; Faidley, L.E. Field-stiffening effect of magneto-rheological elastomers. *Int. J. Solids Struct.* **2013**, *50*, 2281–2288. [CrossRef]
10. Sebald, G.; Nakano, M.; Lallart, M.; Tian, T.; Diguet, G.; Cavaillé, J.Y. Energy conversion in magneto-rheological elastomers. *Sci. Technol. Adv. Mater.* **2017**, *18*, 766–778. [CrossRef] [PubMed]
11. Brancati, R.; Di Massa, G.; Pagano, S.; Santini, S. A magneto-rheological elastomer vibration isolator for lightweight structures. *Meccanica* **2019**, *54*, 333–349. [CrossRef]
12. Zhu, G.; Li, Z.; Guo, H.; Bai, X.F.; Xiong, Y.; Li, M. Dynamic modeling and vibration control for isolation systems based on magnetorheological elastomers. *J. Intell. Mater. Syst. Struct.* **2023**, *34*, 1224–1236. [CrossRef]
13. Lin, D.; Yang, F.; Gong, D.; Li, R. A new vibration isolator integrating tunable stiffness-damping and active driving properties based on radial-chains magnetorheological elastomer. *Mech. Syst. Signal Process.* **2023**, *183*, 109633. [CrossRef]
14. Liu, Q.; Hu, B.; Liu, W.; Li, G.; Chen, Q.; Hu, G. Design and experimental study of a semi-active shear-mode vibration absorber using magnetorheological elastomer. *AIP Adv.* **2024**, *14*, 115223. [CrossRef]
15. Komatsuzaki, T.; Inoue, T.; Terashima, O. Broadband vibration control of a structure by using a magnetorheological elastomer-based tuned dynamic absorber. *Mechatronics* **2016**, *40*, 128–136. [CrossRef]
16. Naito, T.; Terashima, O. Development of the broad band frequency-tunable dynamic absorber using magneto-rheological elastomer for the noise and vibration reduction in mechanical systems. *Adv. Exp. Mech.* **2020**, *5*, 169–177. [CrossRef] [PubMed]
17. Kiyotaki, R.; Ono, K.; Li, Z.; Naito, T.; Terashima, O. Reduction in horizontal and vertical vibrations by dynamic absorber using elliptical shaped magneto-rheological elastomer. *Adv. Exp. Mech.* **2022**, *7*, 123–129. [CrossRef] [PubMed]
18. Den Hartog, J.P. *Mechanical Vibrations*, 4th ed.; McGraw-Hill: New York, NY, USA, 1956.
19. Ormondroyd, J.; Den Hartog, J.P. The theory of the dynamic vibration absorber. *Trans. ASME Appl. Mech.* **1928**, *50*, 9–22.

Disclaimer/Publisher's Note: The statements, opinions and data contained in all publications are solely those of the individual author(s) and contributor(s) and not of MDPI and/or the editor(s). MDPI and/or the editor(s) disclaim responsibility for any injury to people or property resulting from any ideas, methods, instructions or products referred to in the content.